Turbulence statistics in rib-roughened rough-to-smooth (RTS) channel flows

Umair Ismail

Department of Aerospace Engineering
Iowa State University
Ames, Iowa 50011, USA
umair@iastate.edu

Tamer A. Zaki

Department of Mechanical Engineering
Johns Hopkins University
Baltimore, Maryland 21218, USA
t.zaki@jhu.edu

Paul A. Durbin

Department of Aerospace Engineering
Iowa State University
Ames, Iowa 50011, USA
durbin@iastate.edu

ABSTRACT

The effect, after a sudden change in roughness in turbulent channel flows, on mean velocity is not restricted to a so-called internal boundary layer. In fact, the whole vertical extent of the domain experiences local mean acceleration and deceleration that gradually diminishes with the streamwise distance. Although the skin friction re-establishes relatively quickly, turbulence stresses are slow to recover. In the near-wall region, the characteristic smooth-wall cycle re-establishes by $x/\delta \approx 1$ with near-wall peaks in $\overline{u'u'}$ and $\overline{u'v'}$ manifesting immediately. Despite this, complete recovery is exceedingly slow and higher levels of turbulence continue to persist by the domain exit at $x/\delta = 8.33$. On the other hand, the region further away from the wall, i.e. $y^+ > 200$ for $Re_{bulk} = 18000$ in the present context demonstrates an even slower response. Outer-peaks in turbulence stresses reminiscent of the upstream rough-wall gradually decay and move away from the lower wall, eventually almost plateauing-off at significantly higher turbulence levels, i.e. more than 50% of fully developed smooth-wall magnitudes, by the exit of the domain. At this wall-normal height, this response is partly the outcome of non-negligible production rate of turbulence kinetic energy (TKE) and relatively small dissipation rate ε, which although larger than the fully-developed smooth-wall values is not sufficiently large.

INTRODUCTION

Antonia & Luxton (1972) argue that a zero-pressure-gradient turbulent boundary layer over a rough wall adjusts slowly after a step-change in roughness, and this slow response is a feature of both inner and outer layers. However, their near-wall profiles, particularly of turbulence stresses, are of limited resolution due to the experimental techniques used. Recently, Hanson & Ganapathisubramani (2016) showed that for such boundary layers the near-wall peak in the streamwise turbulence stress emerges quickly over the smooth-wall. They verify that for such external flows the internal boundary-layer thickness is a relevant lengthscale above which the flow remains insensitive to the change in boundary condition. However, its importance as a similarity lengthscale for internal flows is still unclear. Further away from the wall, their streamwise turbulence intensity profiles show a somewhat slow yet continuous decay towards the equilibrium levels. Information on additional turbulence stresses and important single-point quantities like the turbulence timescale are hard to measure correctly in physical experiments and are, therefore, missing from their study.

In the present direct numerical simulation (DNS) study, rib-roughness is used to generate fully-developed turbulent flows over a rough wall with the objective to investigate the response of turbulence ultimately towards equilibrium smooth-wall states. Particular attention is paid to mean and turbulence statistics that are crucial from a closure modelling viewpoint. Along with the mean velocity and skin friction behaviour in the transitional regime the relative recovery, rate of recovery and the influence of upstream rough-wall on turbulence stresses in the near-wall region are discussed. This work extends the mean flow and statistical turbulence understanding provided by the aforementioned lab experiments.

SIMULATION PRELIMINARIES

The incompressible Navier-Stokes equations,

$$\frac{\partial u_j}{\partial x_j} = 0, \tag{1}$$

$$\frac{\partial u_i}{\partial t} + \frac{\partial u_i u_j}{\partial x_j} = -\frac{\partial P}{\partial x_i} + \nu \frac{\partial^2 u_i}{\partial x_j \partial x_j}, \tag{2}$$

are solved using the fractional time-step method described in Pierce & Moin (2004). Here, $u_i = \{U,V,W\}$ are the instantaneous velocities in the streamwise, wall-normal and spanwise directions (or $x_i = \{x,y,z\}$), respectively, P is the pressure and ν is the molecular viscosity. This algorithm employs a finite-difference formulation to solve the predictor-corrector equations on a three dimensional staggered cartesian mesh. Second-order central differences are used for all spatial derivatives. A semi-implicit iterative scheme based on Newton-Raphson iterations, that is second-order time accurate, is used to advance the discretized equations in time.

The computational domain is divided into two sections: an initial rough-wall section of length L_{fr} followed by a developing smooth-wall section. A schematic diagram of this computational domain along with the coordinate system used is given in figure 1. Square cylindrical ribs of height k are used to simulate roughness elements on the bottom rough wall, while the upper wall is kept smooth. Like Ikeda & Durbin (2007), a spacing of $w/k = 9$ is used between successive roughness elements. This spacing is wide enough to ensure $k-$type roughness, while providing near-maximum form drag. Downstream plane recycling is used to generate a fully-developed rough-wall regime of length L_{fdr} in the initial

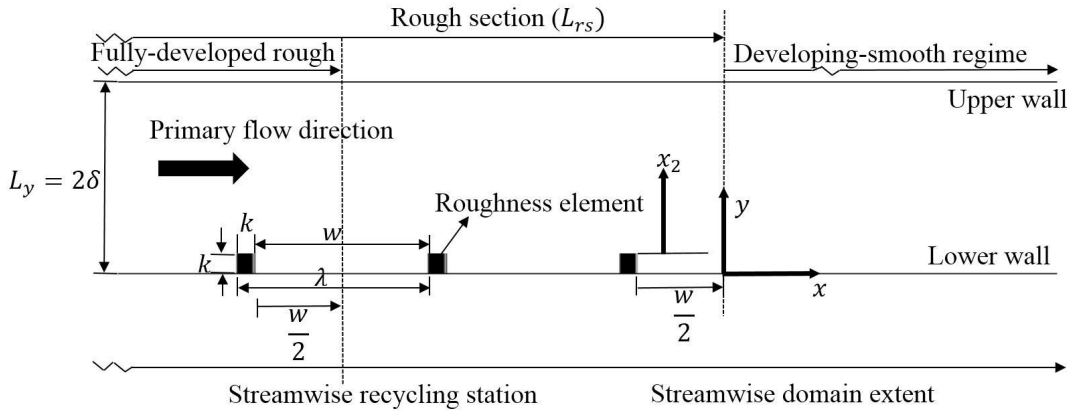

Figure 1: Computational domain and coordinate system. Spanwise (z) direction is outward from the figure.

rough-wall section, and to establish realistic turbulent inflow conditions. The yz recycling station can, alternatively, be thought of as the inflow plane with fully-developed rough-wall inflow conditions for the subsequent downstream developing smooth-wall channel flows. In this study two test cases have been simulated; (A) a low-Reynolds-number case and (B) a high-Reynolds-number case. The parameters of these cases are summarized in table 1.

Jimnez (2004) recommended a $\delta_b/k > 40$ for similarity laws to appear in turbulent rough-wall boundary layers, where δ_b is the boundary layer thickness. However, most laboratory experiments and all direct simulations for rough-wall flows up till now have used much smaller δ/k values. Here, we assume the channel half-height δ and δ_b to be equivalent in order to apply the aforementioned threshold. For their square-rib simulations Leonardi *et al.* (2003) and Miyake *et al.* (2002) used $\delta/k = 5$, while Ikeda & Durbin (2007) used $\delta/k = 8.5$, etc. Ashrafian *et al.* (2004) used a better ratio of $\delta/k \approx 30$, but their simulations were only transitionally rough. Nagano *et al.* (2004) used three different ratios, i.e. $\delta/k = 5, 10$ and 20. Although they did not directly report their effective sand-grain lengthscales, but using the reported k^+ the inferred sand-grain roughness lenghscale for $\delta/k = 20$ was also transitionally rough. Using a $\delta/k \approx 40$, while also properly resolving the numerical grid is prohibitively expensive given the present computational resources. It should be noted that a higher δ/k, although desirable, reduces the effective sand-grain roughness lengthscale r^+ for a given bulk Reynolds number $Re_b = U_b\delta/\nu$, where U_b is the bulk velocity. Therefore the choice of $\delta/k = 12$, while being larger than those used by most previous rough-wall DNS studies, ensures that the fully developed rough-wall regime of our simulations falls in the fully-rough category, i.e $r^+ > 90$ (see Durbin & Reif, 2011). In this fully-rough category, if the roughness geometry is fixed, the flow becomes independent of ν, i.e. the obtained friction velocity at the rough-wall $u_{\tau R}$ becomes independent of Re_b.

Following Antonia & Luxton (1972), the start of the developing smooth-wall regime ($x = 0$) is located at a distance $w/2$ after the last roughness element. Although seemingly arbitrary, this origin is located downstream of the primary re-circulation zone following the last roughness element. Also such a choice means that the rough section has an integer number of roughness-cavities of equal size. For each roughness-cavity the skin friction is calculated using both form drag and viscous drag, whereas in the developing smooth-wall section the skin friction is simply the viscous drag. The no-slip condition is applied at solid boundaries both at the upper and lower walls. Periodic boundary conditions are used in the spanwise direction and the convective outflow condition $\partial u_i/\partial t + c\partial u_i/\partial x = 0$ is applied at the outlet boundary, where c is the local bulk velocity.

Table 2: Spatial and temporal resolutions for the RTS test cases. The normalization is with the friction velocity $u_{\tau S}$ at the upper smooth wall in the fully-developed rough-wall regime.

Case	Δx_s^+	Δz_s^+	$\Delta y_s^+\|_{min}$	$\Delta y_s^+\|_{max}$	Δt_s^+
A	2.35	3.01	0.179	2.46	0.083
B	7.73	8.05	0.436	7.65	0.144

Uniform grid spacing is used in the streamwise and spanwise directions, while a non-uniform grid spacing is used in the wall-normal direction with mesh clustering near the bottom wall, near the top of the roughness elements and near the upper smooth-wall. Stringent restrictions on the spatial resolution are imposed by the initial rough-wall section. The spatial resolution in the present simulations (see table 2) are comparable to that used by Ikeda & Durbin (2007). The simulations are initially advanced for about $50\delta/U_b$ time-units to drive out the transients, after which the calculation of statistics begins and carries on for an additional $250\delta/U_b$ time-units.

RESULTS

Results from three validation simulations are presented in figure 2 to establish confidence in the DNS algorithm. One case is the low-Reynolds-number fully developed smooth-wall channel flow DNS by Moser *et al.* (1999), at $Re_\tau = 180$. The other two cases, that have the same Re_b and a wall-normal domain extent of $L_y = 2\delta + k$, are taken from Orlandi *et al.* (2006). The first of these two cases involves k-type roughness with $\delta/k = 5$ and $w/k = 7$, while the second case comprises of d-type roughness with $w/k = 1$ and the same δ/k ratio. Excellent agreement is obtained with reference data for the smooth-wall channel flow. For the rough-wall validation cases a very good comparison in $\overline{u}$ and $\nu\partial\overline{u}/\partial y$ is achieved as well. Additionally, another case from Leonardi *et al.* (2003) with a spacing similar to that used in the present test cases, $w/k = 9$ (this case has $L_y = 2\delta$), was also simulated. The computed form-drag using their procedure was ~ 0.0122, within 3% of the inferred value from their figure 9.

Fully developed regime Figure 3 shows the inner-scaled mean streamwise velocity profiles at the bottom rough wall in the fully developed regime. The friction velocity at the bot-

Table 1: Summary of simulation parameters from the direct simulations.

Case	Re_b	$L_x/\delta, L_y/\delta, L_z/\delta$	Number of grid points	δ/k	L_{rs}/δ	L_{fdr}/δ	$\Delta t U_b/\delta$
A	4000	$15.83, 2.00, 1.96$	$1900\times326\times192$	12	7.50	5.83	0.0042
B	18000	$15.83, 2.00, 2.08$	$2280\times379\times288$	12	7.50	5.83	0.0021

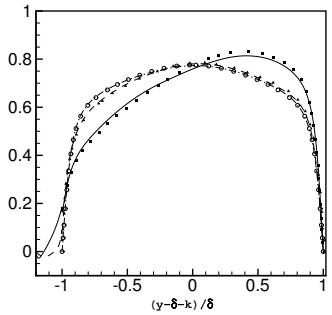

(a)

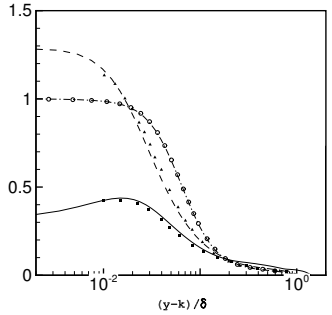

(b)

Figure 2: Validation for fully-developed channel flows: variation in the wall-normal direction of (a) mean streamwise velocity $2\overline{u}/3U_b$ and (b) wall-normal mean velocity gradient $(\nu\partial\overline{u}/\partial y)/u_{\tau C}^2$, where $u_{\tau C}$ is the friction velocity at the wall for the smooth-wall channel flow. ——— rough-wall flow with $w/k=7$ and $k/\delta=0.2$, − − − rough-wall flow with $w/k=1$ and $k/\delta=0.2$, and − · − · − · smooth-wall channel flow with $k/\delta=0$. Filled-symbols: data from Orlandi *et al.* (2006), and open-symbols: data from Moser *et al.* (1999).

tom rough-wall u_{τ_R} is computed using the viscous drag $D_v = (\nu/U_b^2)(1/L_{fdr})\int_0^{L_{fdr}}(\partial\overline{U}/\partial y)|_{y=y^0}dx$ on the bottom wall and top of the roughness elements (the vertical location of these two different types of no-slips surfaces is indicated here by $y=y^0$) and form drag $D_p = (1/U_b^2)(1/L_{fdr})\sum_{n=1}^{N}\int_0^k(\overline{P}_f-\overline{P}_b)dy$ due to the pressure difference across these discrete roughness elements: $u_{\tau R}^2 = D_p + D_v$. In this expression for D_p, N is the number of roughness elements in the fully developed regime, and $\overline{P}_f$ and $\overline{P}_b$ are mean pressure values at front and back of the roughness elements, respectively. Details on the simulation parameters obtained in the fully developed regime are listed in table 3. The two $u_{\tau R}$ values are within 0.2% of each other, thus demonstrating their fully-rough nature. D_v only contributes a very small fraction to the entire $u_{\tau R}^2$, namely 5.5% for case-A and 3.8% for case-B of the from drag D_p, respectively. The form drag D_p contribution remains essentially

Table 3: Parameters obtained in the fully-developed regime. Here the roughness Reynolds number k^+ is defined as $k^+ = u_{\tau R}k/\nu$.

Case	k^+	D_p	D_v	r/δ	r^+
A	42	0.0161	-0.000875	0.694	343
B	185	0.0158	-0.000602	0.694	1540

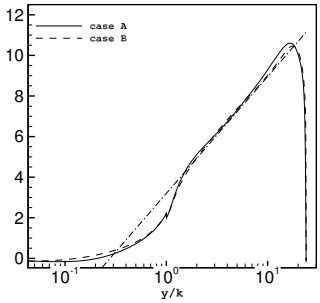

Figure 3: Inner-scaled rough-wall mean streamwise velocity $\overline{U}_R^+$ in the fully-developed regime. The straight line is give by: $\overline{U}_R^+ = (1/0.40)\ln(y/k)+3.2$.

unchanged (less than 2% difference between the two), whereas D_v shows an approximate 30% reduction for the high Re_b simulation (case-B) from case-A. The net contribution of D_v is negative due to the large mean separation bubbles forming both behind of and in front of the roughness elements.

The effective sand-grain roughness lengthscale r is estimated using $r = k\exp[-\kappa(B-8.5)]$, where B is the wall-intercept of the log-law fitted to the inner-scaled mean streamwise velocity profiles. The wall-intercept of the log-law fitted profiles $B=3.2$ is same as that used by Ikeda & Durbin (2007) and Hanjalic & Launder (1972). The effective sand-grain roughness lengthscale r occupies a significant fraction of the channel half-height, $r=0.694\delta$. However, r merely represents a lengthscale that equates the equates the log-layer displacement with the experiments by Nikuradse (1933), and has therefore no actual physical importance to the current setup. Ikeda & Durbin (2007) obtained an effective sand-grain roughness lengthscale $r=1.09\delta$ for their rib-roughened channel flow simulations.

Developing smooth-wall regime The skin friction $C_f = (4\nu/9U_b^2)(\partial\overline{U}/\partial y)$ in the developing smooth-wall regime (see figure 4) is first sharply reduced well below the fully developed smooth-wall levels (gray lines) before recovering and then slowly levelling off (Antonia & Luxton, 1972; Hanson & Ganapathisub-

ramani, 2016). Immediately after the step change in roughness C_f shows negative values due to the large separation bubble following the last roughness element. Case-B indicates almost complete recovery for C_f by $x \approx 2\delta$. Conventional experimental techniques, on the other hand, sometimes suffer from poor estimation of the friction velocity as alluded to by Jacobi & Mckeon (2011), which further leads to uncertainty in inner-scaled profiles. This source of uncertainty is avoided entirely with resolved computer simulations.

Case-A shows a relatively steep increase of C_f compared to case-B. At the start of the developing regime at $x/\delta = 0$, C_f is slightly negative for case-A and slightly positive for case-B. For case-A reattachment for the primary separation bubble behind the last roughness element (RE) occurs at a distance of $4.65k$ downstream of this RE, which lies at $x/\delta > 0$. For case-B the reattachment point is at $4.25k$, which lies at $x/\delta < 0$. By the first streamwise station reported in all the developing smooth-wall figures later, i.e. $x/\delta = 0.42$, C_f for case-A and case-B, respectively, has already recovered to within 17% and 19% of the fully developed smooth-wall channel flow levels.

The mean streamwise velocity $\overline{U}$ in figure 5 shows strong near-wall acceleration immediately following the step change in roughness that slowly decreases in magnitude with downstream distance. The conservation of mass flow rate results in this near-wall acceleration being compensated by deceleration further away from the wall. By the last streamwise station in figure 5, i.e. $x/\delta = 7.1$, the mean velocity, unlike the skin friction, has not recovered completely with $\overline{U}$ showing significant velocity deficit in the lower half of the channel. The outer-scaled mean velocity profiles from figure 5 for the two cases are largely identical to each other, indicating that the recovery of $\overline{U}$ at least from the outer scaling viewpoint is very similar. The point of intersection between two successive and equally spaced streamwise stations from figure 5 divides the mean velocity between regions of local acceleration on the left and local deceleration on the right, and it moves away from the lower-wall with downstream distance in the developing smooth-wall regime. Expectedly due to gradual diminishing of the effect of step-change in roughness with downstream distance, as already observed in C_f profiles above, the difference between these consecutive profiles decreases as well. Furthermore, the presence of mean local acceleration or deceleration in the entire vertical extent of the domain indicates that the influence of this abrupt change in the boundary condition, at least from mean velocity viewpoint, is certainly global and the conventionally used internal layer lengthscale found in literature is of little relevance in the present context.

The streamwise turbulence stress $\overline{u'u'}$ profiles that decay with downstream distance in the developing smooth-wall section are,

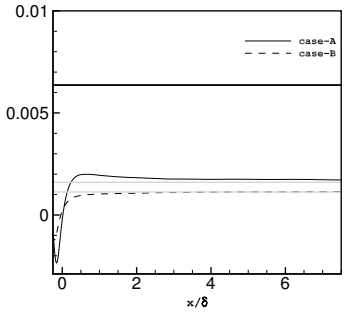

Figure 4: Skin friction C_f profiles in the developing smooth-wall regime. ——— fully developed rough-wall regime, ——— fully developed smooth-wall channel flow.

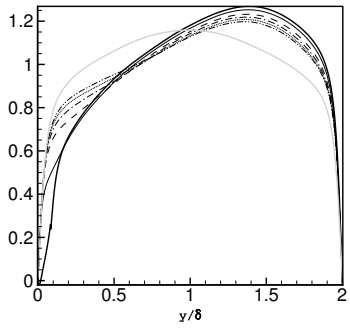

(a) case A

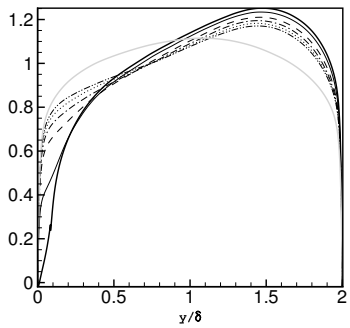

(b) case B

Figure 5: Outer-scaled mean streamwise velocity $\overline{U}/U_b$ in the developing section scaled from the lower wall. ——— in the fully-developed rough regime, ——— at $x/\delta = 0.42$, – – – at $x/\delta = 2.08$, – · – · – at $x/\delta = 3.75$, ····· at $x/\delta = 5.42$, – · · – · · at $x/\delta = 7.08$, ——— from fully-developed smooth-wall channel flow.

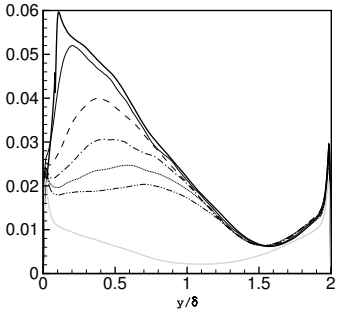

Figure 6: Outer-scaled turbulence streamwise stress $\overline{u'u'}/U_b^2$ for case-B in the developing section scaled from the lower-wall. Lines correspond with figure 5.

for case-B, shown using outer-scaling in figure 6 and using inner-scaling in figure 7. The later figure does not include the fully-developed rough-wall profile because it appears significantly different due to a higher u_τ. The outer peak that is characteristic of the upstream fully-developed rough-wall regime not only decays, but is also transported away from the lower-wall, and by the last streamwise station this outer-peak is only vaguely discernible. The location of the outer-peak in the fully-developed regime persists at $y/\delta \approx 0.11$, or $y/k \approx 1.32$, which is within the $y/\delta = 0.05 - 0.2$

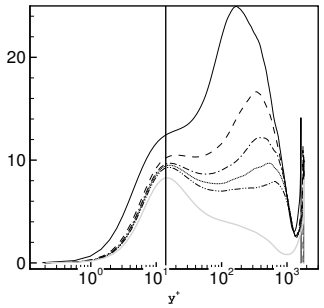

Figure 7: Inner-scaled turbulence streamwise stress $\overline{u'u'}^+$ for case-B in the developing section. The normalization is by the square of friction velocity at the lower-wall. The vertical line identifies the location of the inner-peaks at $y^+ = 14$. Profile labels correspond with figure 5.

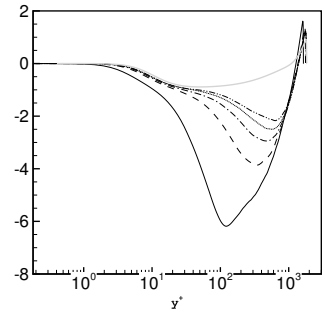

Figure 8: Inner-scaled turbulence shear stress $\overline{u'v'}^+$ for case-B in the developing section. Normalization is by the square of friction velocity at the lower-wall. Lines correspond with figure 5.

range specified for rough-wall boundary layers by Jimnez (2004). In inner coordinates, this outer-peak lies at $y^+ \approx 600$. The wall-normal location of the peak immediately downstream of the roughness as reported by Jacobi & Mckeon (2011) is $y = 0.08\delta = 1.3k$. In terms of roughness length-scale this is consistent with the present observation.

By the second streamwise station as shown in figure 6, $x/\delta \geq 2.08$, the wall-normal gradient of $\overline{u'u'}/U_b^2$ shows a sign change in vicinity of $y/\delta \approx 0.02$ from positive to negative, indicating the establishment of a near-wall peak. This near-wall peak in the buffer-layer at $y^+ \approx 14$ is virtue of the near-wall cycle over the smooth wall. The vertical location of this peak remains essentially fixed at $y^+ \approx 14$, which is comparable to fully developed smooth-wall channel flows of similar Reynolds numbers (see Moser *et al.*, 1999). With downstream distance this inner-peak in figure 7 becomes more distinguished and its magnitude decays and tends towards the smooth-wall levels, but even by the last streamwise station the peak is still about 12% higher than its fully-developed counterpart. Furthermore, instead of also developing much lower levels of $\overline{u'u'}$ near the channel half-height, that are expected of fully-developed smooth-wall channel flows, levels remain high to the last station. Antonia & Luxton (1972) earlier argued that recovery of turbulence stresses in the non-equilibrium region for turbulent boundary layers is slow both very close to the wall and further away from it. The present results in figure 7 clearly demonstrate that this recovery of $\overline{u'u'}$ by the last streamwise station, although slow both very close and further away from the wall, is definitely more complete near the wall, say $y^+ < 30$. This relatively quick recovery near the wall contrasts with the large fluctuations that continue to exist further away from the lower-wall, i.e. $y^+ > 100$.

Like $\overline{u'u'}$, the turbulence shear stress $\overline{u'v'}$ in the fully-developed rough-wall regime also exhibits a single peak and it stays fixed at about $y/\delta \approx 0.095$. Additionally, the downstream evolution of $\overline{u'v'}^+$, as shown in figure 8, also grossly matches the behaviour of $\overline{u'u'}^+$ with comparatively quick near-wall recovery, and the rough-wall peak both decaying and being driven away from the lower wall. By the last streamwise station this rough-wall peak, like for $\overline{u'u'}^+$ is also still discernible. The near-wall peak virtuous of fully-developed smooth-wall flows at $y^+ \approx 30-40$ has been clearly re-established as well, but is being overshadowed by higher turbulence levels and slow recovery further away from the lower-wall.

Between the turbulence streamwise and shear stresses, the relative recovery rate can be compared using an approach similar to the velocity discrepancy method by Jacobi & Mckeon (2011) between

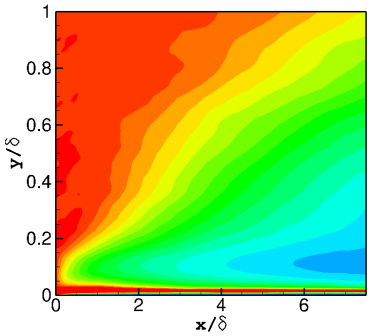

(a)

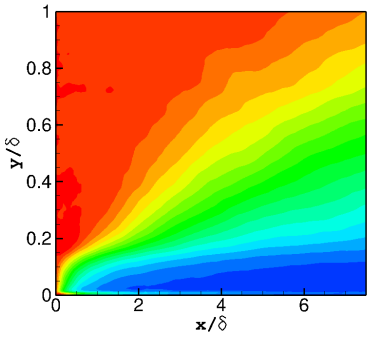

(b)

Figure 9: Normalized recovery magnitudes of turbulence stresses for case-B. (a) $(\overline{u'u'} - \overline{u'u'}_S)/(\overline{u'u'}_R - \overline{u'u'}_S)$, (b) $(\overline{u'v'} - \overline{u'v'}_S)/(\overline{u'v'}_R - \overline{u'v'}_S)$. Scale: blue 0.0, green 0.5, and red 1.0.

perturbed and unperturbed states. We can define recovery magnitudes for different turbulence stresses, which attain a value of 1 at the start of the transitional regime indicated by subscript R, and approach 0 when the fully developed smooth-wall channel flow state indicated by subscript S is achieved. Exact definitions for the two turbulence stresses $\overline{u'u'}$ and $\overline{u'v'}$ are given in figure 9. Clearly the near-wall recovery of $\overline{u'v'}$ progresses more swiftly than $\overline{u'u'}$. The blue stress bubble envelops around one-third of the shown domain, approximately $y/\delta < 0.15$ for the turbulence shear stress; whereas for the streamwise turbulence stress, it has only briefly begun to

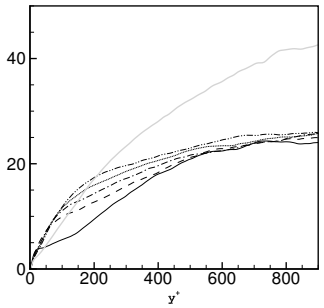

Figure 10: Turbulence time-scale k/ε for case-B. Lines correspond with figure 5.

appear in the region $y/\delta \approx 0.1$ by the exit of the domain.

Another statistic central to turbulence closure modelling is the turbulence timescale k/ε, where k and ε are the turbulence kinetic energy and turbulence dissipation rate, respectively. Figure 10 shows that for $y^+ > 200$, this timescale in the transitional regime is smaller than the fully-developed smooth-wall levels. Even though k for the transitional regime is higher than the fully developed smooth-wall channel flow, much stronger ε persists resulting in a smaller time-scale. Furthermore in the developing-regime at this wall-normal height, k/ε also shows a small increase with downstream distance. This is because although both k and ε primarily decay with x, clearly ε recovers at a relatively faster rate. The recovery of k, on the other hand, is similar to the recovery of $\overline{u'u'}$ as shown in figure 9a. Much closer to the lower-wall, $y^+ < 200$, and after the first streamwise station k/ε shows a momentary increase above the fully-developed smooth-wall levels. With the removal of roughness elements, the roughness induced small-scales disappear instantly resulting in a sharp decrease in ε and hence a subsequent increase in the timescale. However, despite this initial sharp decrease in ε, the eventual reversion of small-scales to their equilibrium fully developed smooth-wall levels is a gradual process that is not entirely complete by the streamwise end of the domain.

Conclusion

We have presented initial results from our ongoing work on using computer simulations to investigate non-equilibrium rough-wall turbulent flows. Results from two separate test cases involving rib-roughened developing rough-to-smooth turbulent channel flows are presented. After the change in boundary condition, the skin friction expectedly undershoots and recovers towards the equilibrium state by at most $x/\delta \approx 2$ for both test cases. The mean velocity and turbulence stresses, however, paint a different picture and have not recovered completely by the end of the domain, $x/\delta = 8.33$. The effect of step-change in roughness as demonstrated by the mean velocity profiles is not restricted to a thin region near the wall, and is felt throughout the limited wall-normal extent of the computational domain. The streamwise and shear turbulence stresses show a comparatively quick recovery close to wall than further away from it, and high levels of turbulence kinetic energy (TKE) continue to persist for $y^+ > 200$ by domain end. This is partly attributed to presence of small but non-negligible streamwise mean shear; additionally, turbulence production and transport rates in the TKE budget equation at this wall-normal height are also comparatively larger than their fully developed smooth-wall equivalents. The timescale k/ε is suppressed in the developing smooth-wall section due to much higher dissipation rate, which is slow to equilibrate even after a rapid initial decrease.

REFERENCES

Antonia, R. A. & Luxton, R. E. 1972 The response of a turbulent boundary layer to a step change in surface roughness. part 2. rough-to-smooth. *Journal of Fluid Mechanics* **53**, 737–757.

Ashrafian, Alireza, Andersson, Helge I. & Manhart, Michael 2004 DNS of turbulent flow in a rod-roughened channel. *International Journal of Heat and Fluid Flow* **25** (3), 373 – 383, turbulence and Shear Flow Phenomena (TSFP-3).

Durbin, Paul A. & Reif, B. A. Pettersson 2011 *Statistical Theory and Modeling for Turbulent Flows*.

Hanjalic, K. & Launder, B. E. 1972 Fully developed asymmetric flow in a plane channel. *Journal of Fluid Mechanics* **51**, 301–335.

Hanson, R. E. & Ganapathisubramani, B. 2016 Development of turbulent boundary layers past a step change in wall roughness. *Journal of Fluid Mechanics* **795**, 494–523.

Ikeda, Tomoaki & Durbin, Paul A. 2007 Direct simulations of a rough-wall channel flow. *Journal of Fluid Mechanics* **571**, 235–263.

Jacobi, I. & Mckeon, B. J. 2011 New perspectives on the impulsive roughness-perturbation of a turbulent boundary layer. *Journal of Fluid Mechanics* **677**, 179–203.

Jimnez, Javier 2004 Turbulent flows over rough walls. *Annual Review of Fluid Mechanics* **36** (1), 173–196.

Leonardi, S, Orlandi, Paolo, Smalley, RJ, Djenidi, L & Antonia, RA 2003 Direct numerical simulations of turbulent channel flow with transverse square bars on one wall. *Journal of Fluid Mechanics* **491**, 229–238.

Miyake, Y., Tsujimoto, K. & Nagai, N. 2002 Numerical simulation of channel flow with a rib-roughened wall*. *Journal of Turbulence* **3**, 035.

Moser, Robert D., Kim, John & Mansour, Nagi N. 1999 Direct numerical simulation of turbulent channel flow up to re=590. *Physics of Fluids* **11** (4).

Nagano, Yasutaka, Hattori, Hirofumi & Houra, Tomoya 2004 DNS of velocity and thermal fields in turbulent channel flow with transverse-rib roughness. *International Journal of Heat and Fluid Flow* **25** (3), 393 – 403, turbulence and Shear Flow Phenomena (TSFP-3).

Nikuradse, J. 1933 Strmungsgesetze in Rauben Rohren. *Verein Deutsher Ingenieure, Forschungsheft* p. 361.

Orlandi, Paolo, Leonardi, S & Antonia, RA 2006 Turbulent channel flow with either transverse or longitudinal roughness elements on one wall. *Journal of Fluid Mechanics* **561**, 279–305.

Pierce, C. D. & Moin, P. 2004 Progress-variable approach for large-eddy simulation of non-premixed turbulent combustion. *Journal of Fluid Mechanics* **504**, 73–97.